Analyst

Accepted Manuscript

This article can be cited before page numbers have been issued, to do this please use: J. Popp, E. Farnesi, M. Calvarese, C. Liu, C. Messerschmidt, M. S. Vafaeinezhad, T. Meyer, D. Cialla-May, C. Krafft, J. Ballmaier, O. Guntinas-Lichius and M. Schmitt, *Analyst*, 2024, DOI: 10.1039/D4AN00868E.




ROYAL SOCIETY OF CHEMISTRY

rsc.li/analyst

View Article Online
DOI: 10.1039/D4AN00868E

ARTICLE

# Advancing cerumen analysis: exploring innovative vibrational spectroscopy techniques with respect their potential as new point-of-care diagnostic tool

Received 00th January 20xx,
Accepted 00th January 20xx

DOI: 10.1039/x0xx00000x

Edoardo Farnesi[a,b‡], Matteo Calvarese[b‡], Chen Liu[a,b], Carl Messerschmidt[b], Mohammad Sadegh Vafaeinezhad[a], Tobias Meyer-Zelder[b], Dana Cialla-May[b], Christoph Krafft[b], Jonas Ballmaier[c], Orlando Guntinas-Lichius[c], Michael Schmitt[a] and Jürgen Popp[a,b]

Cerumen, commonly known as earwax, is a complex mixture composed of secretions from ceruminous glands. These secretions are known as heterogeneous mixture mainly composed of lipids and proteins. Despite its prevalence, the potential diagnostic value of cerumen remains largely unexplored. Here, we present an in-depth analysis of cerumen utilizing well-known vibrational approaches like conventional Raman spectroscopy or surface enhanced Raman spectroscopy (SERS) together with advanced vibrational spectroscopy techniques such as coherent Raman scattering (CRS) approaches, i.e. broadband coherent anti-Stokes Raman scattering (CARS) or stimulated Raman scattering (SRS), and moreover Optical PhotoThermal InfraRed (OPTIR) spectroscopy. Through the integration of these vibrational spectroscopic methods, lipids and proteins could be identified as the main components of cerumen; however, they contribute to a various extent to the final spectral information depending on the vibrational detection scheme applied. The inherent weak Raman signal could be enhanced by linear (SERS) and non-linear (CRS) processes resulting in efficient acquisition of fingerprint information and allowing for the detection of marker modes, which cannot be addressed by conventional Raman. OPTIR provides complementary information to Raman spectroscopy, however, without the contribution of a fluorescence background. Our findings underscore the utility of these cutting-edge techniques in unveiling the intricate molecular landscape of cerumen, paving the way for novel point-of-care diagnostic methodologies and therapeutic interventions.

## Introduction

In point-of-care personalized medicine, accurately detecting diseases in early stages is one of the crucial challenges. Prompt diagnosis gives rise to successful and rapid therapy, which surely improves the prognosis of a patient, with higher probability of surviving and also better life quality.

The quest for a progress in point-of-care diagnostics has seen a recent boost in the branch of liquid biopsy, which seeks to provide a valid and reliable essay of diagnosing and identifying illness from body-fluids [1,2]. Since any change in homeostatic balance alters the human health status, the analysis of biological fluids mirrors in a fast, reliable and non-invasive manner what is occurring inside an affected body. Moreover, these point-of-care trials result of pivotal importance as some disease-associate biomarkers can be found in peripheral biomatrices at the very early stage of pathology when successful therapies and the improvement of patient survivability are much more likely [3]. Numerous studies have been conducted over the past decades on countless diseases, especially cancer, exploring clinically relevant body-fluids for the detection and follow-up of pathologies such as oral cancer [4], pancreatic cancer [5], lung cancer [6], ovarian cancer [7], and breast cancer [8]. Point-of-care biomarkers tests from non-blood fluids (e.g. saliva, urine, stool, tears, sweat, breath, seminal fluid, cerumen) are not for all of these matrices available and needs more research before translation into clinical routine procedures [9].

Cerumen, a yellowish waxy substance often overlooked, plays a crucial role in the auditory canal's health and functionality. Composed of a heterogeneous mixture of lipids (including saturated and unsaturated fatty acids, 60 – 70 %), proteins (high percentage of keratin, 20 – 30 %), and other organic compounds, cerumen serves as a protective barrier, shielding the delicate structures of the ear canal from foreign particles, pathogens, and water [10–15]. Apart from the forensic context, i.e. post-mortem drug overdose and alcohol abuse evaluations, in clinical diagnostics, this body-fluid has not been valorized enough over time, but only in a few cases. In diagnosis of some metabolic diseases, as allergic rhinitis and otosclerosis, some genetic disorder, as maple syrup urine disease and alkaptonuria, and only recently breast cancer and some cancer biomarkers, were detected by testing earwax [16,17].

Despite being a neglected body-fluid, cerumen is hardly prone to ambient air and/or cosmetics contamination and most importantly, the access is easy, the sampling is painless and non-invasive, with a

[a] Institute of Physical Chemistry (IPC) and Abbe Center of Photonics (ACP), Friedrich Schiller University Jena, Member of the Leibniz Centre for Photonics in Infection Research (LPI), Helmholtzweg 4, 07743 Jena, Germany.
[b] Leibniz Institute of Photonic Technology, Member of Leibniz Health Technologies, Member of the Leibniz Centre for Photonics in Infection Research (LPI), Albert-Einstein-Straße 9, 07745 Jena, Germany.
[c] Department of Otorhinolaryngology-Head and Neck Surgery, Jena University Hospital, 07747 Jena, Germany.
‡These authors contributed equally
Supplementary Information available: [details of any supplementary information available should be included here]. See DOI: 10.1039/x0xx00000x

View Article Online
DOI: 10.1039/D4AN00866B



storage time longer than other bio-matrices as saliva, urine and serum [18].

Traditional methods of cerumen analysis have primarily focused on physical characteristics such as color, texture, and odor, offering limited insights into its biochemical composition and potential diagnostic significance.

In recent years, vibrational spectroscopy has emerged as a powerful tool for the non-invasive, label-free analysis of biological samples, enabling detailed molecular characterization with high sensitivity and specificity. Here, we explore to the best of our knowledge for the first time the potential of a multitude of different vibrational spectroscopic techniques in analyzing and characterizing cerumen based on its unique vibrational spectroscopic signatures. In detail we apply Raman spectroscopy (RS), Surface-enhanced Raman spectroscopy (SERS), Broadband Coherent Anti-Stokes Raman spectroscopy (BCARS), Stimulated Raman scattering (SRS) and Optical Photothermal Infrared spectroscopy (OPTIR) to characterize human cerumen samples. These vibrational spectroscopy techniques are invaluable in a wide range of bioanalytical applications, including disease diagnosis and fundamental biological research [19–21]. RS provides molecular vibrational information, allowing for the identification and characterization of various biomolecules [22,23]. However, the inherent weak Raman signal can sometimes be overwhelmed by background noise, limiting its sensitivity. SERS, on the other hand, overcomes the weak signal intensity of traditional Raman spectroscopy. By leveraging the electromagnetic enhancement of plasmonic nanoparticles, SERS greatly enhances the Raman signal from analytes adsorbed on the nanoparticle surface. Additionally, a chemical enhancement mechanism is observed in SERS, being the minor contribution to the overall SERS enhancement. The SERS technique has been extensively used to detect trace amounts of biological molecules, enabling sensitive and selective analysis with potential applications in diagnostics and therapeutics [24,25]. BCARS and SRS are nonlinear Raman methods that provide an alternative approach to enhance the Raman signal from weak scatterers, making them suitable for the study of biological samples. Both BCARS and SRS have proven to be valuable tools for studying lipid metabolism, drug delivery, and other cellular processes, being able to visualize lipid droplets, lipoproteins, and other lipid-rich structures [26–29]. OPTIR is a technique that measures the absorption, reflection, and transmission of infrared light to identify specific functional groups (such as hydroxyl, carbonyl, and amide bonds present in lipids, proteins, and carbohydrates) in biomolecules, providing detailed information about molecular structures, hydrogen bonding, and conformational changes [30,31].

Comparing the outputs from RS, SERS, BCARS, SRS and OPTIR, and leveraging the unique strengths of each spectroscopic technique, we aim to unravel the complex molecular architecture of cerumen, shedding light on its biological functions and diagnostic implications. This first comprehensive vibrational spectroscopic study of cerumen aims to advance the frontier for the development of new clinical diagnosis methods using a non-invasive and easily collected biomatrix.

## Materials and Methods

### 1. Cerumen sample preparation

Cerumen samples (Fig. 1) were collected from two healthy individuals. This study was approved by the Jena University Hospital Ethics Committee (RAMTUMAR study; no. 2021-2305-Material), and all volunteers provided written informed consent for enrolling in this study. By limiting our investigation to two specimens, we were able to focus on carefully characterizing the collected spectra, ensuring that any observed patterns or anomalies could be confidently attributed to the inherent properties of the cerumen rather than to inter-sample variability.

Around 50-100 mg of earwax from both ears of each individual were collected in the hospital without damaging the ear canal and immediately stored at -80° C until vibrational spectroscopic analysis. Through visible inspection, only samples with no sign of blood contamination were used for measurement. After thawing at room

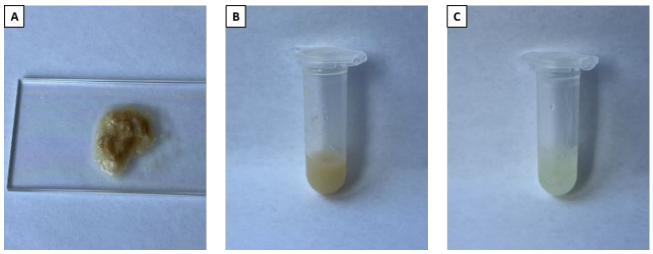


*Figure 1. Cerumen specimens analyzed by means of vibrational techniques. A) human semi-solid cerumen on a microscope glass slide. B) Human liquid cerumen after pre-processing preparation, i.e. supernatant. C) Artificial cerumen.*

temperature, cerumen samples were both analyzed directly in their typical sticky semi-solid condition and in liquid condition, after solubilization. For this pre-processing part, the samples were transferred to 1.5 mL centrifuge tube and 0.5 mL of PBS was added in the tube, following an established procedure from the literature.[32,33] After 1 h of sonication at 36 °C, the samples were centrifuged at 13000 g for 10 min and then each supernatant was transferred in a new tube, ready for the measurements.

Human earwax has been compared with artificial cerumen (Pickering Laboratories, Mountain View, CA, USA) representing the lipid secretion of the natural cerumen. It contains oleic acid (20% w/w), linoleic acid (20% w/w), lanolin (20% w/w), paraffin oil (10% w/w), palmitic acid (20% w/w), myristic acid (20% w/w).

For RS measurements, semi-solid, artificial and liquid cerumen samples were placed on a silicon chip, while for CARS, SRS and OPTIR analyses a microscope glass slide was used as the substrate (as illustrated in Fig. 1A).

For SERS analysis, both silver (Ag)-coated and gold (Au)-coated silicon nanopillar substrates (SERStrates™), purchased from Silmeco ApS (Copenhagen, Denmark) were incubated in liquid cerumen within the tubes for 20 min. After incubation, each SERS chip was placed on a microscope glass slide and left to dry slowly at room temperature, thus favoring the leaning process of the vertically oriented and highly packed (~20 pillars/$\mu m^2$) nanopillars thanks to the surface tension.

### 2. Raman and SERS

RS and SERS measurements were performed using a WITec alpha300 R confocal Raman microscope (Ulm, Germany) equipped with a 785 nm laser as excitation source. The Raman scattered light was collected with a 10× objective lens. RS spectra were collected in the range of 600 to 3100 $cm^{-1}$, using a laser power incident on the sample of 50 mW, a 300 grooves/mm grating and an integration time of 5 s with one accumulation. The acquisition was performed over a 2 × 2 $mm^2$ area in the middle of the deposited sample with a 50-point map (5 points per line, 10 lines per scan).

Setting the laser power on the sample to 5 mW, SERS spectra were recorded with the same Raman instrumentation as described before, within the range of 600 to 2200 $cm^{-1}$, using a 600 groove/mm grating, 10x objective lens, and an integration time of 5 s with one accumulation. The acquisition was performed over a 1.5 × 1.5 $mm^2$ area in the center of the chip with a 150-point map (15 points per line, 10 lines per scan).

Spectral analysis was performed with Origin Pro 2022 (OriginLab, Northampton, MA, USA) software. After removing possible outliers, which show spectral features such as sharp spikes or strong fluorescence background signals, Raman and SERS raw spectra, were processed with baseline correction (fifth-order polynomial fit), smoothing, and normalization by area (see Figure S1 and S2 for the background-corrected Raman and SERS spectra). Mean intensity profiles were obtained for each sample. Band assignment was conducted based on data from the literature[34–37].

**3. BCARS and SRS**

A home built BCARS spectroscopy platform was used to acquire broadband CARS spectra. The setup, shown in Figure S3, employs a multiplex CARS approach in which a narrowband pump pulse at 1032 nm and a broadband Stokes pulse ranging from about 1100 nm to nearly 1600 nm are superimposed on the sample to generate a broadband anti-Stokes signal, containing Raman-spectral information between 700 and 3200 $cm^{-1}$. A complete description of the setup is included in the Supplementary Information and Figure 4A illustrates a simplified diagram of the setup. Broadband CARS spectra of the liquid, semi-solid and artificial cerumen were acquired using an average power of 15 mW for the pump and 2 mW for the Stokes at the sample plane, at a repetition rate of 1 MHz. A 20x/NA 0.4 objective lens was applied.

To prevent photodamage on the specimens, the laser focus was scanned on the sample and an image was acquired, with a pixel acquisition time of 20 ms over a 50x50 $\mu m^2$ field of view. To remove the inherently present non-resonant background (NRB)[38] a Kramers-Kronig (KK) phase retrieval algorithm was employed [39,40]. Before processing, the BCARS images were processed by K-means clustering and the cluster of spectra with highest intensity were averaged. The KK algorithm was then applied to the average spectrum of each sample using a mean BCARS spectrum of the glass slide as the reference NRB.

Stimulated Raman Scattering (SRS) spectra of the three samples (see Figure 1) were acquired using a commercial multimodal microscopy platform (Stellaris 8, Leica Microsystems GmbH). The microscope is equipped with a SRS detection scheme and enables the acquisition of broadband SRS spectra in a hyperspectral configuration, i.e. the Stokes wavelength is fixed, and the pump wavelength is sequentially scanned. The system features a CARS and SRS excitation laser (picoEmerald, A.P.E. GmbH) that provides a Stokes pulse at about 1031 nm and a tunable pump pulse in the 700-990 nm range at a repetition frequency of 80 MHz. For SRS acquisition, the Stokes pulse is modulated at 20 MHz and a lock-in detection scheme is employed. Figure 4 B illustrates the schematics of the setup.

The three samples (see Figure 1) were measured by acquiring images over a field of view of 1.55 x 1.55 $mm^2$, with 512 x 512 pixels, 3.16 µs pixel acquisition time and using a 10x/NA 0.40 objective (HC PL APO CS2 DRY) for excitation. In the 900-1800 $cm^{-1}$ wavenumber range, the power was set to about 12 mW for the pump and 29 mW for the Stokes. In the CH stretching wavenumber region, due to high signal intensity, the power was reduced to around 4 mW and 8.5 mW for the pump and Stokes pulses, respectively.

K-means clustering was performed on the SRS images to group and average only the spectra with the highest intensity. Being a background-free technique, no further processing, apart for fifth-order polynomial fit baseline, was required to retrieve Raman spectral information from the SRS signal.

Figure S4 and S5 show the raw SRS spectra after K-means clustering and the BCARS spectra after clustering and NRB removal. The SRS spectra clearly show greater variability in the data, which can be attributed to several factors. These include high heterogeneity of the sample surface in the wide FOV, low signal due to sample thickness and short pixel dwell time, and low spatial sampling (more information is provided in the Supplementary Information).

**4. OPTIR**

OPTIR spectra and images of cerumen presented in this work were performed with the mIRage + R™ Infrared microscope (Photothermal Spectroscopy Corp., Santa Barbara, CA, USA), controlled by the PTIR Studio software. The instrument is equipped with a four-chip pulsed and broadly tunable high-power quantum cascade laser (QCL) covering the spectral ranges 934-1800 $cm^{-1}$ and 2700 to 2999 $cm^{-1}$ (MIRcat 2400, Daylight) and a 785 nm probe laser (Cobolt). Spectral and imaging data were collected in reflection mode by focusing the IR laser on the sample using a 40 × /NA 0.78 reflective Cassegrain-style objective. The power of the QCL IR laser was set to 21% at a 10% duty cycle and the power of the probe laser to 37%. Cerumen samples were deposited on microscope glass slides. OPTIR spectra at a resolution of 6.6 $cm^{-1}$ were acquired in high-speed mode at 1000 $cm^{-1}$/s with two averages. All spectra were automatically normalized to the collected background spectrum as displayed in Figure S6. Discrete wavenumber OPTIR images were recorded from 70×70 µm

View Article Online DOI: 10.1039/D4AN00868E

*Table 1. Comparison of the capabilities and characteristics of the different spectroscopic techniques.*

| Technique | Acquisition speed | Setup / Level of maturity | Background | Quantitative analysis |
|---|---|---|---|---|
| Raman | 5 s / spectrum | Commercial system / High | Fluorescence | Possible and well established |
| SERS | 5 s / spectrum | Commercial system and commercial substrates / High | Fluorescence | Limited reproducibility |
| Hyperspectral SRS | 5 s / spectral point | Commercial system / Medium | None | Possible[42] |
| Multiplex Broadband CARS | 20 ms / spectrum | Custom-made system / Low | Non-resonant background | Limited due to nonlinear dependence on concentration |
| OPTIR | 2 s / spectrum | Commercial system / Medium | None | Possible[30] |

region of interest with 70 µm/s speed and 1 µm step size at 2850 and 1650 $cm^{-1}$. DC images record the intensity of the probe laser reflection which mimics white light images.

**5. Comparison of the measurement techniques**

Table 1 compares the different vibrational spectroscopy techniques used in this study to highlight the strengths and weaknesses of each, especially from the perspective of point-of-care analysis of earwax, or body fluids in general. The “Acquisition speed” refers to that used for measurements in this study. The "Setup/Level of maturity" column indicates whether the spectra were acquired with a commercial or homemade setup and what is the level of maturity of the technique. "Background" indicates whether the techniques inherently show a background signal that must be removed by post-processing to recover spectral information. “Quantitative analysis" deals with the possibility of performing quantitative analysis on the chemical composition of samples under examination. It mainly relates to the linearity of the techniques with respect to concentration of chemical species and their reliability and reproducibility. Since the SRS hyperspectral cube is generated by sequential sweeping of each wavenumber, it is not possible to directly calculate the acquisition time of a spectrum. The table shows the sweeping time required to tune the wavelength, given on the official excitation laser documentation page (https://www.ape-berlin.de/en/cars-srs/#specification). Laser wavelength tuning time is the limiting factor in hyperspectral SRS, as the actual exposure time can be on the order of ms as for BCARS. Laser systems designed specifically for SRS can achieve a much smaller sweeping time than our system, as low as 5 ms [41]. The QCL is also tuned at a speed to 1000 $cm^{-1}$ per second to collect IR spectra which gives minimum collection time of ca. 2 sec.

## Results and discussion

**1. Raman spectroscopy as vibrational spectroscopic gold standard for the identification of potential diagnostic biomarkers in cerumen**

RS represents a powerful tool for biomolecular analysis. In this section we report, to the best of our knowledge for the first time, about the vibrational characteristics of human semi-solid, human liquid and artificial cerumen by means of RS. Fig. 2 shows spontaneous Raman spectra of all earwax specimens depicted in Fig. 1 deposited on silicon wafers. All spectra highlight to a large degree lipid contributions both in fingerprint and high wavenumber regions with the most prominent bands at 2940, 2888, 2856, 1450, and 1298, 1125 and 1060 $cm^{-1}$. Table 2 provides a detailed band assignment as well as the respected references.

At high wavenumbers, the $CH_2$ symmetric stretching vibration of lipids results in the most intensive peak at 2856 $cm^{-1}$ followed by Fermi resonance of the $CH_2$ deformation overtone at 2888 $cm^{-1}$ and anti-symmetric $CH_2$ stretching at 2940 $cm^{-1}$ of lipids and smaller contributions of proteins, respectively. In the fingerprint region, the main Raman peaks are assigned to the $CH_2$ scissoring (1450 $cm^{-1}$), and $CH_2$ in phase twisting (1298 $cm^{-1}$) due to lipids. Symmetric and asymmetric C-C modes of fatty acids chain show bands at 1060 and 1125 $cm^{-1}$, respectively. Unsaturated fatty acids chains are evident from C=CH (1265 $cm^{-1}$) and C=C (1658 $cm^{-1}$) vibrations. Weaker molecular vibrations typical of proteins show up only in semi-solid cerumen spectrum, in particular a shoulder near 1004 $cm^{-1}$ (phenylalanine) and 1658 $cm^{-1}$ (amide I) which slightly broadens the C=C band of lipids. Furthermore, β-carotenoids (1156 and 1536 $cm^{-1}$) modes are detected in semi-solid cerumen (see Fig. 2 red spectrum).The lipid unsaturation degree can be calculated as the ratio of Raman bands intensities at 1660 and 1450 $cm^{-1}$.[43] Altered

View Article Online
DOI: 10.1039/D4AN00858E



secretions of lipids have considerable diagnostic relevance, especially in cancer diagnostics. Increased lipid metabolism results the most substantial tumor metabolic defect. Abnormal lipid synthesis contributes to fast cancer cell growth and tumorigenesis, in fact an increasing number of studies underscores that cancers depend on fatty acid and lipid supply.[44,45] These molecular Raman spectroscopic signatures of cerumen might be used as future possible pre- or post-operative diagnostic and prognostic tools in cancer liquid biopsies. The detection of pathological alterations in

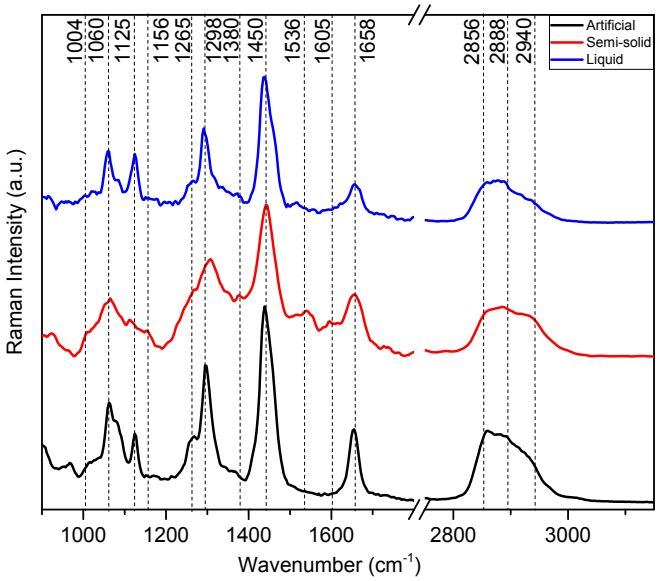


*Figure 2. Averaged Raman spectra of earwax samples displayed in Fig. 1. Artificial cerumen (black spectrum), human semi-solid cerumen (red spectrum) and human liquid cerumen (blue spectrum). Wavenumber range between 900-3100 cm-1. The spectra are cut between the (1800 and 2750 cm-1). Spectra are offset for clarity.*

lipids and proteins through RS relies on changes in the intensity ratio of specific aforementioned Raman peaks associated with these biomolecules. Changes within this unique Raman spectroscopic fingerprint might therefore allow for the identification of molecular signatures indicative of various diseases and pathological conditions within cerumen. Pathophysiological variations in lipids are often accompanied by changes in their relative abundance, composition, and structural properties. These alterations manifest itself in the Raman spectra as shifts in the intensity ratio of characteristic Raman peaks corresponding to lipid and protein vibrational modes (see Table 2), reflecting underlying biochemical changes associated with disease progression. These changes in Raman intensity ratios may be attributed to variations in lipid synthesis or the presence of disease-specific biomarkers within earwax samples.

For instance, previous studies showed that RS serves as a valuable tool for detecting lipids and providing insight into their composition and distribution in various pathological conditions, including brain tumors, breast cancer and atherosclerotic plaques. These diseases are commonly characterized by the accumulation of lipids, particularly cholesterol and triglycerides[46–48]. While it presents several advantages, such as non-destructive analysis, chemical specificity, and minimal sample preparation, RS also faces limitations related to signal intensity and possible fluorescence interference. Weak signals, especially for diluted analytes or low-concentration biomarkers in complex biological fluids, limit the detection sensitivity and acquisition speed. Indeed, the Raman spectral analysis of liquid cerumen (blue spectrum Fig. 2) droplets reveals very weak proteins Raman signals in the fingerprint wavenumber region. To overcome this limitation, the use of advanced Raman signal enhancement techniques or coherent amplification strategies shows a great potential to improve the detection sensitivity of biomarker for a possible point-of-care diagnosis. Recent advancements in SERS and CRS have propelled the field beyond the capabilities of traditional RS.

## 2. Boosting the Raman spectroscopic efficiency with plasmonic and coherent enhancement techniques

### 2.1 SERS analysis

SERS can achieve Raman signal enhancements of several orders of magnitude, effectively overcoming the intrinsic limitations of conventional Raman spectroscopy mentioned above. This increased sensitivity enables the detection of trace-level analytes in complex matrices, surpassing the detection limits of spontaneous Raman spectroscopy by a significant margin.

Here, we performed a SERS analysis of earwax for liquid and artificial cerumen absorbed on Ag-coated and Au-coated silicon nanopillars as SERS substrates. These SERS substrates (purchased from Silmeco ApS, Copenhagen, Denmark) have been chosen due to their high sensitivity. More details about this potent SERS substrate can be found in literature [49,50].

As shown in the SEM images (Figure 3 A-B), the leaning mechanism after air-drying process induces silicon nanopillars to pull together, trapping the cerumen molecules in the hot-spots. Having the analytes localized in several hot spots result pivotal for a significant enhancement of earwax Raman signal due to the coupling effect of localized surface plasmon resonances between close nanopillars [49].

To observe uniform SERS signals, spectra were collected in the central area of the leaned nanopillars chips. Figure 3 C-D shows a deformation and skeletal CC stretching of amino acids. The SERS signal at 1004 $cm^{-1}$ is characteristic for the ring breathing mode of phenylalanine, and the band at 1130 $cm^{-1}$ for lipid CC stretching of fatty acids[51]. The SERS peaks at 1325 and 1586 $cm^{-1}$ are due to the $CH_2$ in-phase twisting and C=C out-phase stretching of amino acids/lipids, respectively. Moreover, protein amide I (1623 $cm^{-1}$) and C=C in-phase stretching (1682 $cm^{-1}$) vibrations of lipids are also visible. In comparison to the artificial cerumen (Figure 3 C, black line), no distinct vibrational pattern was detected as we observed for liquid

View Article Online
DOI: 10.1039/D4AN00868E

cerumen from healthy volunteers. One explanation could be that the diagnostic tumor markers (i.e. epithelial and oral cancers) but

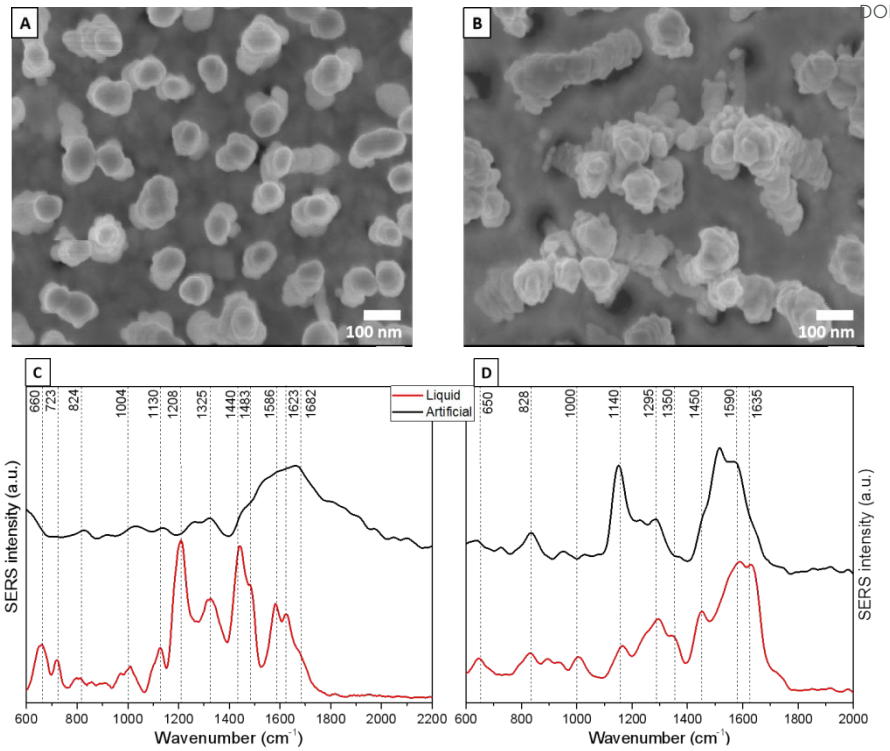


*Figure 3. SEM images of Ag-coated silicon nanopillars substrates A) before and B) after their leaning mode due to drying process. Averaged SERS spectra of artificial (black) and liquid (red) cerumen absorbed respectively on C) Ag-coated and D) Au-coated coated SERS substrates. Spectral range 600-2000 cm$^{-1}$. Spectra are offset for clarity.*

chemical composition is varying between these two sample classes and moreover, due to the viscous properties of artificial cerumen, the leaning effect of the Ag nanopillars is less pronounced and thus, the mean SERS spectra show less intensity, resulting in biochemical feature assignment only in the 1500-1700 cm$^{-1}$ region.

On the other side, the artificial cerumen SERS spectrum absorbed on Au nanopillars (Figure 3D, black line) helps to identify fatty acids (i.e. palmitic acid) through the characteristic peaks at 1140 cm$^{-1}$ (C-C stretching), 1295 cm$^{-1}$ ($CH_2$ in-phase twisting) and 1590 cm$^{-1}$ (C=C out-phase stretching). Other prominent SERS peaks in liquid cerumen (Figure 3 D, red line) are assigned to protein amide I (1635 cm$^{-1}$), protein/lipid CH deformation or $CH_2$/$CH_3$ bending (1450 cm$^{-1}$) and protein CH wagging (1350 cm$^{-1}$). The SERS peaks appearing at 650, 828 and 1000 cm$^{-1}$ are assigned to amino acids $COO^-$ deformation, amino acids C-C stretching and aromatic amino acids ring breathing vibrations, respectively.

Overall, this band assignment shows that cerumen SERS analysis highlights the possible detection of vibrational contributions from two well-known biomarkers traditionally used as point-of-care diagnostic and prognostic tools, namely lipid acids and keratins via the SERS bands at 1586 and 1140 cm$^{-1}$ for the fatty acid, and 1623, 1350 and 660 cm$^{-1}$ for the protein, respectively. Palmitic acid, as well as keratin which are playing a key role in anti-inflammatory processes and regulation of lipid metabolism, are cancer biomarker in neuroblastoma, breast cancer and oral cancer [52,53]. Keratins, with their altered levels in blood, are also extensively recognized as increasing evidence have been reported in their role as prognostic markers and as active regulators of tumorigenesis [54].

This difference between the cerumen SERS spectra collected using Ag-coated and Au-coated substrates means that specific biochemical components of cerumen that having stronger affinity with either Au or Ag nanopillars dominate the respective spectra, leading to the stark differences observed. These interactions analytes/metal surfaces can cause shifts in peak positions, changes in intensity as well as their ratio, and even the appearance or disappearance of certain vibrational modes, contributing further to the disparity between the SERS spectra obtained from the two metals.

### 2.2 BCARS and SRS analysis

Coherent Raman scattering (CRS) in a single-wavenumber configuration has emerged in recent decades as a powerful tool for rapid, label-free imaging of biological media by exploiting the vibrational information of a single characteristic Raman peak of large intensity. Its broadband configurations, namely broadband CARS (BCARS) and broadband SRS, combine the high acquisition speed of CRS with the high spectral information content provided by Raman scattering. In this section, we show the BCARS and broadband SRS spectral characterization of liquid and semi-solid human cerumen and artificial cerumen. The difference between these two techniques mainly lies in how the Raman spectroscopic information is detected. In the BCARS process, the anti-Stokes scattered signal is collected and spectrally unmixed by a conventional spectrograph. In

View Article Online
DOI: 10.1039/D4AN00885E

hyperspectral SRS, specifically in the setup we utilize, the small change in the pump intensity (Stimulated Raman Loss) is observed by a complex lock-in detection scheme. A multiplex BCARS approach, like the setup we implemented, allows for fast acquisition with exposure times in the order of ms even for biologically relevant samples [55]. SRS acquisition speed, on the other hand, strongly relies on the wavelength tunability speed of the excitation laser. Faster multiplex SRS approaches with multi-channel lock-in platforms have been already developed but are still limited to few spectral channels [56].

in the detected SRS intensity depends linearly on concentration, thus allowing for greater sensitivity at lower concentrations and possible quantitative analysis similar to that of spontaneous Raman spectroscopy [42].

The spectral analysis of cerumen recorded by the BCARS and SRS setups depicted in Figures 4A and B show the potential of these vibrational techniques to detect lipids, especially in the high wavenumber region. Consistent with the Raman spectra in Figure 2, spectral contributions of proteins are weak. Here, BCARS spectra (Figure 4C) highlight the possibility to trace unsaturated fatty acids

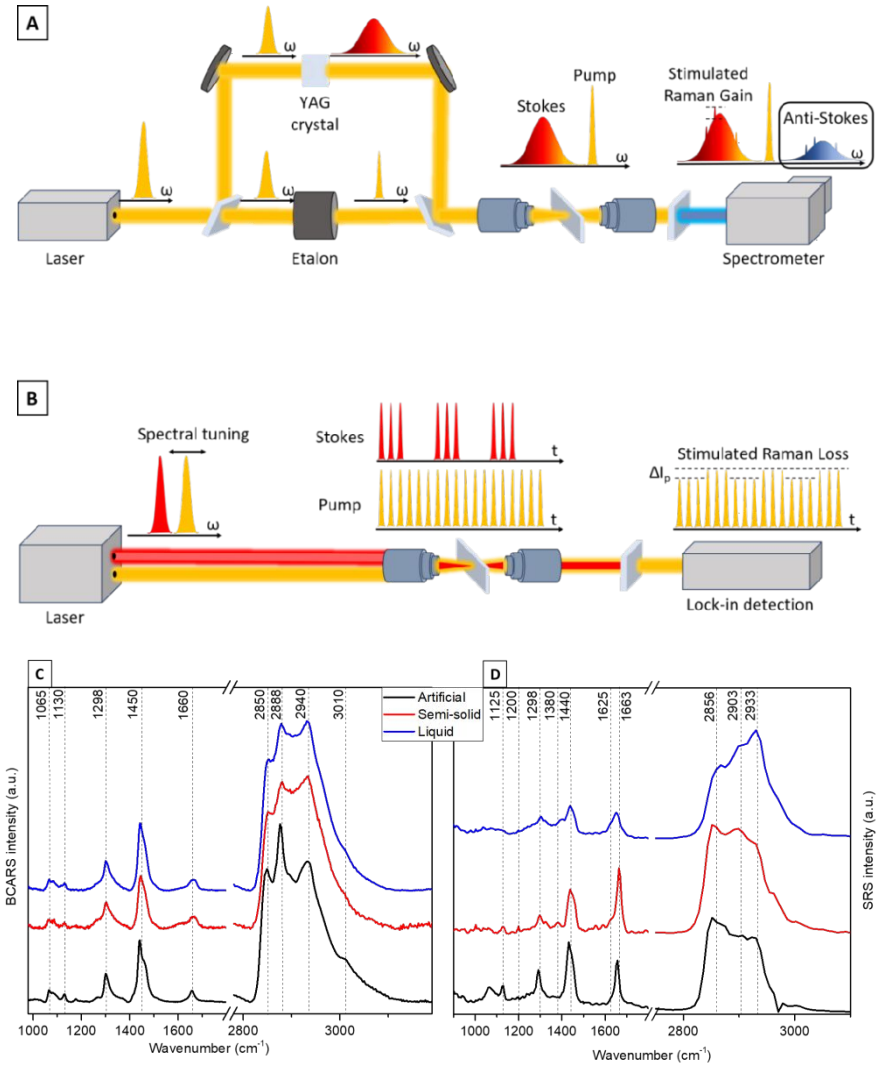


*Figure 4. Schematic illustrations of the A) home-build BCARS and B) SRS setups. Averaged C) BCARS and D) SRS spectra of artificial (black), semi-solid (red) and liquid (blue) cerumen. Wavenumber range between 900-3200 cm$^{-1}$. The spectra are cut between in the silent region (1800 and 2750 cm$^{-1}$). Spectra are offset for clarity.*

Despite the slower speed and greater complexity of the detection scheme, SRS provides a background-free signal that needs no further processing, whereas BCARS requires advanced computational techniques to eliminate the non-resonant four-wave-mixing background. Furthermore, while the BCARS signal shows a quadratic dependence on the density of scatterers in the sample, the variation

present in human cerumen through the characteristic bands of C=C stretching vibration at 1660 cm$^{-1}$ and the =CH stretching vibration at 3010 cm$^{-1}$, making possible a detection of saturated and unsaturated lipids. Moreover, the relative intensity ratio by CARS signals belonging to lipid $CH_2$ and protein $CH_3$ stretching modes (2888 and 2940 cm$^{-1}$), suggest a clear traceability of protein-to-lipid variations in the human liquid media [57].

View Article Online
DOI: 10.1039/D4AN00865E



The same spectral trend is detectable for the same characteristic vibrational bands in SRS measurements (Figure 4D), where the peak at 2933 $cm^{-1}$ results in the highest intensity. SRS also allows evaluating the lipid content around 2850 $cm^{-1}$, a typical band of the $CH_2$ symmetrical stretching vibration highly abundant in lipids. In the fingerprint wavenumber region, which is dominated by lipids peaks at 1440 and 1663 $cm^{-1}$, the human earwax SRS spectra also show some peaks assigned to the COH in-plane bending vibration at 1380 $cm^{-1}$ that point to sphingoglycolipids[34]. Both SRS and BCARS probe mainly fatty acids contributions. The analysis of the BCARS and SRS fingerprint region shows comparable spectral profiles than the Raman spectra plotted in Figure 2, but acquired in a much shorter measurement time (as mentioned in Table 1).

### 3. OPTIR analysis as complementary tool

The Raman analysis presented above shows that Raman spectroscopy mainly displays molecular vibrations of non-polar biomolecules. IR absorption spectroscopy might complement the Raman analysis by also highlighting molecular vibrations exhibiting a large dipole moment like e.g. hydroxyl, carbonyl, and amide bonds present in lipids, proteins, and carbohydrates. Usually, the application of IR spectroscopy to native biomedical specimens is hindered due to the presence of water. In this context OPTIR in combination with IR quantum cascade laser offers a solution for also studying aqueous biomedical samples. OPTIR offers high-resolution, non-invasive analysis and contrast of non-transparent biological samples in reflection on ordinary glass windows as compared to the commonly applied IR approach FT-IR.

Here we have also applied OPTIR to study human semi-solid, human liquid and artificial cerumen to obtain Raman complementary information about the biomolecular cerumen composition.

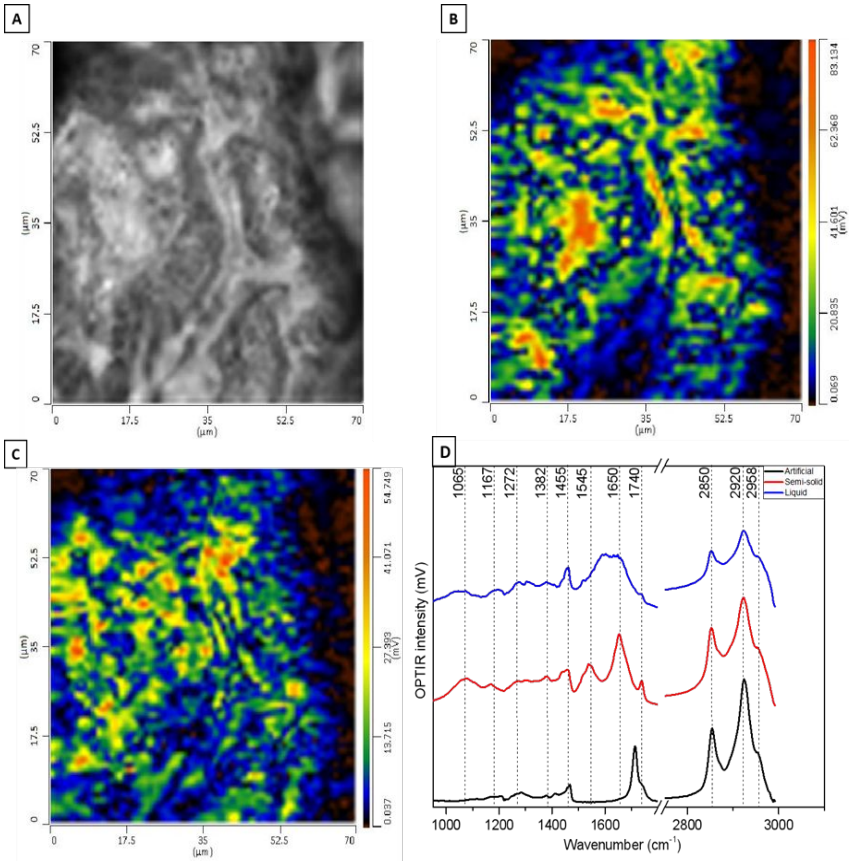


*Figure 5. OPTIR images of semi-solid cerumen. A) DC image. B) Lipid distribution: $v_{as}(CH_2)$(2850 $cm^{-1}$). C) Protein distribution: amide I (1650 $cm^{-1}$). D) OPTIR spectra of artificial (black), semi-solid (red) and liquid (blue) cerumen. Spectral range between 900-3000 $cm^{-1}$. The silent region (1800 and 2700 $cm^{-1}$) is not covered by the QCL tuning range. Spectra are offset for clarity.*

Figure 5 shows DC and OPTIR hyperspectral images of human semi-solid earwax. The OPTIR imaging mode allows to explore with high resolution the spatial heterogeneity of the sample by setting the IR laser to two fixed wavenumbers. Here we have chosen the $CH_2$ symmetric stretching vibration at 2850 $cm^{-1}$ of lipids (Figure 5 B) and the amide I vibration at 1650 $cm^{-1}$ of proteins (Figure 5 C). Evidencing the predominant and homogeneous distribution of lipids, OPTIR maps also reveal some protein-rich spots.

A representative OPTIR spectrum of semi-solid cerumen in Figure 5D (red line) clearly shows the amide II and amide I bands at 1545 and 1650 $cm^{-1}$. The band at 1065 $cm^{-1}$ is typical for COH groups[58] which

supports the detection of sphingoglycolipids in SRS spectra (Figure 4D). The lipid C=O stretching band is found at 1740 $cm^{-1}$ in semi solid cerumen and is shifted towards lower wavenumbers for artificial cerumen. The amide bands of proteins are untypically broad, and the C=O band is weak in liquid cerumen. Only typical $CH_2$ bands at 1455 (deformation mode) and 2850/2920 $cm^{-1}$ (stretching modes) are properly resolved and are evident also in the other cerumen OPTIR spectra. (Table 2). Some of these vibrational contributions have already been reported by Elkins [59], in a cerumen study through ATR-FTIR spectroscopy. However, OPTIR leads to superior identification and lateral resolution capabilities, especially for inhomogeneous specimens.

**4. Discussion**

Table 2 summarizes the afore-presented vibrational spectroscopic cerumen analysis. Main spectral contributions in all samples with all modalities were assigned to lipids, in particular $CH_2$ stretching vibrations in the high wavenumber range. Raman marker bands indicate the degree of unsaturation of fatty acids chains. Raman and IR marker bands of COH groups point to sphingoglycolipids that are made up of fatty acid chains and a ceramide backbone linked to saccharine residues such as galactose. Furthermore, Raman spectra detect typical bands of carotenoids. IR spectra detect amide bands of proteins that are much weaker in Raman spectra. An indirect detection of lipid to protein variations can be achieved by the ratio of $CH_2$ and $CH_3$ stretching vibrations in the high wavenumber range. Protein bands seem to be enhanced in SERS spectra relative to lipid bands. The SERS spectra differ from those obtained using conventional Raman, CARS, SRS, and OPTIR techniques due to the fundamentally distinct principles underlying these methods. Conventional Raman spectroscopy, for example, directly measures vibrational modes based on the inelastic scattering of monochromatic light, without requiring enhancement mechanisms. This results in spectra that reflect the bulk properties of the sample rather than being dominated by surface interactions, as is the case with SERS. In contrast, SERS amplifies the Raman signal of molecules in close proximity to the metal surface, leading to a more surface-specific and often highly sensitive detection of molecular species that might otherwise be undetectable in bulk Raman measurements. This surface selectivity can result in SERS spectra that enhance different vibrational modes or molecular species compared to those observed in conventional Raman spectra. Additionally, CARS and SRS, which are nonlinear Raman techniques, involve the coherent interaction of multiple laser beams to generate the Raman signal. While these techniques offer high spatial resolution and the ability to selectively probe specific vibrational modes, they operate based on principles that differ from those of SERS.

*Table 2. Tentative band assignment for the spectra acquired by the different techniques. as - asymmetric, s - symmetric, ν - stretching, δ - deformation, β - in plane bending, τ - in phase twisting. AAs – amino acids.*

| RS | Ag SERS | Au SERS | BCARS | SRS | OPTIR | BAND ASSIGNMENTS |
|---|---|---|---|---|---|---|
| | | | 3010 | | | ν(=CH) unsaturated lipids[34,35] |
| 2940 | | | 2940 | 2930 | 2958 | $\nu_{as}(CH_3)$ proteins/lipids[34,35] |
| | | | | | 2920 | $\nu_{as}(CH_2)$ lipids[34,35] |
| 2888 | | | 2888 | 2903 | | Fermi resonance $\delta(CH_2)$ lipids[34,35] |
| 2856 | | | 2850 | 2856 | 2850 | $\nu_{s}(CH_2)$ lipids[34,35] |
| | | | | | 1740 | ν(C=O) esters lipids[34,35] |
| 1658 | 1623 | 1635 | 1660 | 1660 | 1650 | ν(C=C) lipids/ amide I proteins[36] |
| | 1586 | 1590 | | | | proteins[34,35] |
| 1536 | | | | | 1545 | Raman: carotenoids / IR: amide II |
| 1445 | 1440 | 1450 | 1450 | 1440 | 1455 | $\delta(CH_{2/3})$ lipids /proteins[36] |
| 1380 | | | | 1380 | 1382 | β(COH) sphingoglycolipids[34] |
| | 1325 | 1350 | | | | protein AAs[36,37] |
| 1298 | 1325 | 1295 | 1298 | 1298 | 1272 | $\tau(CH_2)$ lipids /amide III proteins[34,35] |
| | 1208 | | | 1200 | | proteins[36] |

| | | | | | | |
|---|---|---|---|---|---|---|
| 1156 | | | | | | carotenoids[34] |
| 1125 | 1130 | 1140 | 1130 | 1125 | | ν(C-C) lipids [34,35] |
| 1060 | | | 1065 | | 1065 | ν(CC) or β(COH) sphingoglycolipids [34,35] |
| | 1004 | 1000 | | | | protein AAs [36,37] |
| | 824 | 828 | | | | protein AAs [36,37] |
| | 723 | | | | | Protein AAs [36] |
| | 660 | 650 | | | | Protein AAs [36] |

View Article Online
DOI: 10.1039/D4AN00868E



The combination of the advanced vibrational spectroscopy techniques may offer a multimodal point-of-care approach enhancing diagnostic capabilities and enabling comprehensive characterization of body-fluids in general. Raman spectroscopy is well established to collect the full molecular fingerprint. Challenges in terms of sensitivity may arise for low concentrated molecules and molecules with inherent fluorescent emission overlapping with weaker Raman signals. SERS, in the fingerprint wavenumber region, provides higher detection sensitivity and enables trace-level analysis of specific biomarkers in cerumen media. For the high wavenumber region, SRS and especially BCARS offer unparalleled capabilities for molecular analysis, allowing to possibly detect variations in lipid and protein content which is essential information for diagnostic and prognostic tools in cancer liquid biopsies. OPTIR is a variant of IR spectroscopy that gives complementary information to Raman-based methods. Benefits of OPTIR spectroscopy and imaging include data acquisition in reflection mode, sample preparation on inexpensive glass slides, images with submicrometer resolution and spectra with minimal background and comparable to established FTIR spectroscopy of thin films or thick samples in attenuated total reflection mode.

## Conclusions

Multiple vibrational spectroscopy techniques were applied offering a powerful approach for the comprehensive analysis of cerumen and shedding light on its complex molecular composition and biological significance. By leveraging the unique strengths of the used vibrational spectroscopic approaches, we uncovered the molecular signatures embedded within cerumen, paving the way for innovative diagnostic methodologies and therapeutic interventions. The insights gained from this interdisciplinary study not only enhance our understanding of cerumen biology but also highlight the potential of vibrational spectroscopy in biomedical research and clinical practice.

The primary goal was to obtain preliminary data that would either support or refute the hypothesis that vibrational spectroscopy could serve as a viable diagnostic approach for cerumen analysis. The successful application of these techniques to the two healthy samples has provided encouraging results, offering a solid basis for future research that will systematically investigate cerumen samples from a broader population, including those with various health conditions. Ultimately, this study marks the initial step in a promising investigation, setting the stage for more comprehensive research that will assess the clinical utility of vibrational spectroscopy in diagnosing and monitoring health conditions through cerumen analysis. As technology continues to advance, vibrational spectroscopy is poised to revolutionize point-of-care diagnostics, transforming healthcare delivery, and improving patient outcomes worldwide.

## Author contributions

The manuscript was written through contributions of all authors. Conceptualization, E.F., M.C. and M.S.; Sampling and sample preparation: E.F., M.C., J.B. and C.L.; investigation, E.F., M.C., C.M. and M.S.V.; supervision, D.C.-M. and T.M-Z.; writing—original draft preparation, E.F. and M.C.; writing—review and editing, C.K., O.G.-L., M.S., D.C.-M., and J.P.; funding acquisition, O.G.-L., M.S., and J.P. / All authors have given approval to the final version of the manuscript. / ‡These authors contributed equally.

## Conflicts of interest

There are no conflicts to declare. The authors declare that they have no known competing financial interests or personal relationships that could have appeared to influence the work reported in this paper.

## Data availability

The data supporting this article have been included as part of the Supplementary Information.

## Acknowledgements

The work presented has received funding from the European Union's Horizon research and innovation programme under grant

agreements No. 101016923 (CRIMSON), No. 860185 (PHAST) and No. 101135175 (uCAIR).

## References

(1) Liu, D.; Wang, J.; Wu, L.; Huang, Y.; Zhang, Y.; Zhu, M.; Wang, Y.; Zhu, Z.; Yang, C. Trends in Miniaturized Biosensors for Point-of-Care Testing. *TrAC Trends in Analytical Chemistry* **2020**, *122*, 115701. https://doi.org/10.1016/j.trac.2019.115701.

(2) Soda, N.; Rehm, B. H. A.; Sonar, P.; Nguyen, N.-T.; Shiddiky, M. J. A. Advanced Liquid Biopsy Technologies for Circulating Biomarker Detection. *J Mater Chem B* **2019**, *7* (43), 6670–6704. https://doi.org/10.1039/C9TB01490J.

(3) Palmirotta, R.; Lovero, D.; Cafforio, P.; Felici, C.; Mannavola, F.; Pellè, E.; Quaresmini, D.; Tucci, M.; Silvestris, F. Liquid Biopsy of Cancer: A Multimodal Diagnostic Tool in Clinical Oncology. *Ther Adv Med Oncol* **2018**, *10*, 175883591879463. https://doi.org/10.1177/1758835918794630.

(4) Zhang, X.; Li, B. Updates of Liquid Biopsy in Oral Cancer and Multiomics Analysis. *Oral Dis* **2023**, *29* (1), 51–61. https://doi.org/10.1111/odi.14064.

(5) Qi, Z.-H.; Xu, H.-X.; Zhang, S.-R.; Xu, J.-Z.; Li, S.; Gao, H.-L.; Jin, W.; Wang, W.-Q.; Wu, C.-T.; Ni, Q.-X.; Yu, X.-J.; Liu, L. The Significance of Liquid Biopsy in Pancreatic Cancer. *J Cancer* **2018**, *9* (18), 3417–3426. https://doi.org/10.7150/jca.24591.

(6) Di Capua, D.; Bracken-Clarke, D.; Ronan, K.; Baird, A.-M.; Finn, S. The Liquid Biopsy for Lung Cancer: State of the Art, Limitations and Future Developments. *Cancers (Basel)* **2021**, *13* (16), 3923. https://doi.org/10.3390/cancers13163923.

(7) Bhardwaj, B. K.; Thankachan, S.; Venkatesh, T.; Suresh, P. S. Liquid Biopsy in Ovarian Cancer. *Clinica Chimica Acta* **2020**, *510*, 28–34. https://doi.org/10.1016/j.cca.2020.06.047.

(8) Alba-Bernal, A.; Lavado-Valenzuela, R.; Domínguez-Recio, M. E.; Jiménez-Rodriguez, B.; Queipo-Ortuño, M. I.; Alba, E.; Comino-Méndez, I. Challenges and Achievements of Liquid Biopsy Technologies Employed in Early Breast Cancer. *EBioMedicine* **2020**, *62*, 103100. https://doi.org/10.1016/j.ebiom.2020.103100.

(9) Paluszkiewicz, C.; Pięta, E.; Woźniak, M.; Piergies, N.; Koniewska, A.; Ścierski, W.; Misiołek, M.; Kwiatek, W. M. Saliva as a First-Line Diagnostic Tool: A Spectral Challenge for Identification of Cancer Biomarkers. *J Mol Liq* **2020**, *307*, 112961. https://doi.org/10.1016/j.molliq.2020.112961.

(10) Feig, M. A.; Hammer, E.; Völker, U.; Jehmlich, N. In-Depth Proteomic Analysis of the Human Cerumen—A Potential Novel Diagnostically Relevant Biofluid. *J Proteomics* **2013**, *83*, 119–129. https://doi.org/10.1016/j.jprot.2013.03.004.

(11) Coon, A. M.; Setzen, G.; Musah, R. A. Mass Spectrometric Interrogation of Earwax: Toward the Detection of Meniere's Disease. *ACS Omega* **2023**, *8* (30), 27010–27023. https://doi.org/10.1021/acsomega.3c01943.

(12) Coon, A. M.; Dane, A. J.; Setzen, G.; Cody, R. B.; Musah, R. A. Two-Dimensional Gas Chromatographic and Mass Spectrometric Characterization of Lipid-Rich Biological Matrices–Application to Human Cerumen (Earwax). *ACS Omega* **2022**, *7* (1), 230–239. https://doi.org/10.1021/acsomega.1c04535.

(13) Prokop-Prigge, K. A.; Thaler, E.; Wysocki, C. J.; Preti, G. Identification of Volatile Organic Compounds in Human Cerumen. *Journal of Chromatography B* **2014**, *953–954*, 48–52. https://doi.org/10.1016/j.jchromb.2014.01.043.

(14) Guest, J. F.; Greener, M. J.; Robinson, A. C.; Smith, A. F. Impacted Cerumen: Composition, Production, Epidemiology and Management. *QJM* **2004**, *97* (8), 477–488. https://doi.org/10.1093/qjmed/hch082.

(15) Schwaab, M.; Hansen, S.; Gurr, A.; Schwaab, T.; Minovi, A.; Sudhoff, H.; Dazert, S. Protein Isolation from Ear Wax Made Easy. *European Archives of Oto-Rhino-Laryngology* **2009**, *266* (11), 1699–1702. https://doi.org/10.1007/s00405-009-0960-5.

(16) Shokry, E.; Filho, N. R. A. Insights into Cerumen and Application in Diagnostics: Past, Present and Future Prospective. *Biochem Med (Zagreb)* **2017**, *27* (3). https://doi.org/10.11613/BM.2017.030503.

(17) Barbosa, J. M. G.; Pereira, N. Z.; David, L. C.; de Oliveira, C. G.; Soares, M. F. G.; Avelino, M. A. G.; de Oliveira, A. E.; Shokry, E.; Filho, N. R. A. Cerumenogram: A New Frontier in Cancer Diagnosis in Humans. *Sci Rep* **2019**, *9* (1), 11722. https://doi.org/10.1038/s41598-019-48121-4.

(18) Chiang, S. P.; Lowry, O. H.; Senturia, B. H. Micro-chemical Studies on Normal Cerumen I. The Lipid and Protein Content of Normal Cerumen as Affected by Age and Sex. *Laryngoscope* **1955**, *65* (10), 927–934. https://doi.org/10.1288/00005537-195510000-00002.

(19) Mitchell, A. L.; Gajjar, K. B.; Theophilou, G.; Martin, F. L.; Martin-Hirsch, P. L. Vibrational Spectroscopy of Biofluids for Disease Screening or Diagnosis: Translation from the Laboratory to a Clinical Setting. *J Biophotonics* **2014**, *7* (3–4), 153–165. https://doi.org/10.1002/jbio.201400018.

(20) Beć, K. B.; Grabska, J.; Huck, C. W. Biomolecular and Bioanalytical Applications of Infrared Spectroscopy – A Review. *Anal Chim Acta* **2020**, *1133*, 150–177. https://doi.org/10.1016/j.aca.2020.04.015.

(21) Dumont, E.; De Bleye, C.; Sacré, P.-Y.; Netchacovitch, L.; Hubert, P.; Ziemons, E. From Near-Infrared and Raman to Surface-

Enhanced Raman Spectroscopy: Progress, Limitations and Perspectives in Bioanalysis. *Bioanalysis* **2016**, *8* (10), 1077–1103. https://doi.org/10.4155/bio-2015-0030.

(22) Pappas, D. Raman Spectroscopy in Bioanalysis. *Talanta* **2000**, *51* (1), 131–144. https://doi.org/10.1016/S0039-9140(99)00254-4.

(23) Cialla-May, D.; Krafft, C.; Rösch, P.; Deckert-Gaudig, T.; Frosch, T.; Jahn, I. J.; Pahlow, S.; Stiebing, C.; Meyer-Zedler, T.; Bocklitz, T.; Schie, I.; Deckert, V.; Popp, J. Raman Spectroscopy and Imaging in Bioanalytics. *Anal Chem* **2022**, *94* (1), 86–119. https://doi.org/10.1021/acs.analchem.1c03235.

(24) Tahir, M. A.; Dina, N. E.; Cheng, H.; Valev, V. K.; Zhang, L. Surface-Enhanced Raman Spectroscopy for Bioanalysis and Diagnosis. *Nanoscale* **2021**, *13* (27), 11593–11634. https://doi.org/10.1039/D1NR00708D.

(25) Vázquez-Iglesias, L.; Stanfoca Casagrande, G. M.; García-Lojo, D.; Ferro Leal, L.; Ngo, T. A.; Pérez-Juste, J.; Reis, R. M.; Kant, K.; Pastoriza-Santos, I. SERS Sensing for Cancer Biomarker: Approaches and Directions. *Bioact Mater* **2024**, *34*, 248–268. https://doi.org/10.1016/j.bioactmat.2023.12.018.

(26) Krafft, C.; Schmitt, M.; Schie, I. W.; Cialla-May, D.; Matthäus, C.; Bocklitz, T.; Popp, J. Label-Free Molecular Imaging of Biological Cells and Tissues by Linear and Nonlinear Raman Spectroscopic Approaches. *Angewandte Chemie International Edition* **2017**, *56* (16), 4392–4430. https://doi.org/10.1002/anie.201607604.

(27) Çulha, M. Raman Spectroscopy for Cancer Diagnosis: How Far Have We Come? *Bioanalysis* **2015**, *7* (21), 2813–2824. https://doi.org/10.4155/bio.15.190.

(28) Fan, Y.; Wang, S.; Zhang, F. Optical Multiplexed Bioassays for Improved Biomedical Diagnostics. *Angewandte Chemie* **2019**, *131* (38), 13342–13353. https://doi.org/10.1002/ange.201901964.

(29) Freudiger, C. W.; Min, W.; Saar, B. G.; Lu, S.; Holtom, G. R.; He, C.; Tsai, J. C.; Kang, J. X.; Xie, X. S. Label-Free Biomedical Imaging with High Sensitivity by Stimulated Raman Scattering Microscopy. *Science (1979)* **2008**, *322* (5909), 1857–1861. https://doi.org/10.1126/science.1165758.

(30) Sandt, C.; Borondics, F. Super-Resolution Infrared Microspectroscopy Reveals Heterogeneous Distribution of Photosensitive Lipids in Human Hair Medulla. *Talanta* **2023**, *254*, 124152. https://doi.org/10.1016/j.talanta.2022.124152.

(31) Shaik, T. A.; Ramoji, A.; Milis, N.; Popp, J.; Krafft, C. Optical Photothermal Infrared Spectroscopy and Discrete Wavenumber Imaging for High Content Screening of Single Cells. *Analyst* **2023**, *148* (22), 5627–5635. https://doi.org/10.1039/D3AN00902E.

(32) Meier, S. I.; Koelzer, S. C.; Schubert-Zsilavecz, M.; Toennes, S. W. Analysis of Drugs of Abuse in Cerumen - Correlation of Postmortem Analysis Results with Those for Blood, Urine and Hair. *Drug Test Anal* **2017**, *9* (10), 1572–1585. https://doi.org/10.1002/dta.2177.

(33) Massadeh, A. M.; Al-Rawi, N. H.; Fayyad, M. T.; Shotar, A. M.; Al-Farras, M. I.; A Massadeh, S. A. Simultaneous Determination of Tramadol in Earwax and Urine Samples: Effects of Age, Duration Time and Sex. *Bioanalysis* **2024**, *16* (6), 363–374. https://doi.org/10.4155/bio-2023-0217.

(34) Krafft, C.; Neudert, L.; Simat, T.; Salzer, R. Near Infrared Raman Spectra of Human Brain Lipids. *Spectrochim Acta A Mol Biomol Spectrosc* **2005**, *61* (7), 1529–1535. https://doi.org/10.1016/j.saa.2004.11.017.

(35) Rygula, A.; Majzner, K.; Marzec, K. M.; Kaczor, A.; Pilarczyk, M.; Baranska, M. Raman Spectroscopy of Proteins: A Review. *Journal of Raman Spectroscopy* **2013**, *44* (8), 1061–1076. https://doi.org/10.1002/jrs.4335.

(36) Farnesi, E.; Rinaldi, S.; Liu, C.; Ballmaier, J.; Guntinas-Lichius, O.; Schmitt, M.; Cialla-May, D.; Popp, J. Label-Free SERS and MD Analysis of Biomarkers for Rapid Point-of-Care Sensors Detecting Head and Neck Cancer and Infections. *Sensors* **2023**, *23* (21), 8915. https://doi.org/10.3390/s23218915.

(37) Bruzas, I.; Lum, W.; Gorunmez, Z.; Sagle, L. Advances in Surface-Enhanced Raman Spectroscopy (SERS) Substrates for Lipid and Protein Characterization: Sensing and Beyond. *Analyst* **2018**, *143* (17), 3990–4008. https://doi.org/10.1039/C8AN00606G.

(38) Polli, D.; Kumar, V.; Valensise, C. M.; Marangoni, M.; Cerullo, G. Broadband Coherent Raman Scattering Microscopy. *Laser Photon Rev* **2018**, *12* (9). https://doi.org/10.1002/lpor.201800020.

(39) Liu, Y.; Lee, Y. J.; Cicerone, M. T. Broadband CARS Spectral Phase Retrieval Using a Time-Domain Kramers–Kronig Transform. *Opt Lett* **2009**, *34* (9), 1363. https://doi.org/10.1364/OL.34.001363.

(40) Camp, C. H.; Lee, Y. J.; Cicerone, M. T. Quantitative, Comparable Coherent Anti-Stokes Raman Scattering (CARS) Spectroscopy: Correcting Errors in Phase Retrieval. *Journal of Raman Spectroscopy* **2016**, *47* (4), 408–415. https://doi.org/10.1002/jrs.4824.

(41) Brinkmann, M.; Fast, A.; Hellwig, T.; Pence, I.; Evans, C. L.; Fallnich, C. Portable All-Fiber Dual-Output Widely Tunable Light Source for Coherent Raman Imaging. *Biomed Opt Express* **2019**, *10* (9), 4437. https://doi.org/10.1364/BOE.10.004437.

(42) Manifold, B.; Fu, D. Quantitative Stimulated Raman Scattering Microscopy: Promises and Pitfalls. *Annual Review of Analytical Chemistry* **2022**, *15* (1), 269–289. https://doi.org/10.1146/annurev-anchem-061020-015110.

(43) Rosales-Solano, H.; Galievsky, V.; Murtada, K.; Radovanovic, P. V.; Pawliszyn, J. Profiling of Unsaturated Lipids by Raman Spectroscopy Directly on Solid-Phase Microextraction Probes. *Anal Chem* **2022**, *94* (2), 606–611. https://doi.org/10.1021/acs.analchem.1c04054.

(44) Xiong, Y.; Si, Y.; Feng, Y.; Zhuo, S.; Cui, B.; Zhang, Z. Prognostic Value of Lipid Metabolism-related Genes in Head and Neck Squamous Cell Carcinoma. *Immun Inflamm Dis* **2021**, *9* (1), 196–209. https://doi.org/10.1002/iid3.379.

(45) Schmidt, J.; Kajtár, B.; Juhász, K.; Péter, M.; Járai, T.; Burián, A.; Kereskai, L.; Gerlinger, I.; Tornóczki, T.; Balogh, G.; Vígh, L.; Márk, L.; Balogi, Z. Lipid and Protein Tumor Markers for Head and Neck Squamous Cell Carcinoma Identified by Imaging Mass Spectrometry. *Oncotarget* **2020**, *11* (28), 2702–2717. https://doi.org/10.18632/oncotarget.27649.

(46) Köhler, M.; Machill, S.; Salzer, R.; Krafft, C. Characterization of Lipid Extracts from Brain Tissue and Tumors Using Raman Spectroscopy and Mass Spectrometry. *Anal Bioanal Chem* **2009**, *393* (5), 1513–1520. https://doi.org/10.1007/s00216-008-2592-9.

(47) Hanna, K.; Krzoska, E.; Shaaban, A. M.; Muirhead, D.; Abu-Eid, R.; Speirs, V. Raman Spectroscopy: Current Applications in Breast Cancer Diagnosis, Challenges and Future Prospects. *Br J Cancer* **2022**, *126* (8), 1125–1139. https://doi.org/10.1038/s41416-021-01659-5.

(48) You, A. Y. F.; Bergholt, M. S.; St-Pierre, J.-P.; Kit-Anan, W.; Pence, I. J.; Chester, A. H.; Yacoub, M. H.; Bertazzo, S.; Stevens, M. M. Raman Spectroscopy Imaging Reveals Interplay between Atherosclerosis and Medial Calcification in the Human Aorta. *Sci Adv* **2017**, *3* (12). https://doi.org/10.1126/sciadv.1701156.

(49) Schmidt, M. S.; Hübner, J.; Boisen, A. Large Area Fabrication of Leaning Silicon Nanopillars for Surface Enhanced Raman Spectroscopy. *Advanced Materials* **2012**, *24* (10). https://doi.org/10.1002/adma.201103496.

(50) Morelli, L.; Zór, K.; Jendresen, C. B.; Rindzevicius, T.; Schmidt, M. S.; Nielsen, A. T.; Boisen, A. Surface Enhanced Raman Scattering for Quantification of *p* -Coumaric Acid Produced by *Escherichia Coli*. *Anal Chem* **2017**, *89* (7), 3981–3987. https://doi.org/10.1021/acs.analchem.6b04428.

(51) Shen, L.; Du, Y.; Wei, N.; Li, Q.; Li, S.; Sun, T.; Xu, S.; Wang, H.; Man, X.; Han, B. SERS Studies on Normal Epithelial and Cancer Cells Derived from Clinical Breast Cancer Specimens. *Spectrochim Acta A Mol Biomol Spectrosc* **2020**, *237*, 118364. https://doi.org/10.1016/j.saa.2020.118364.

(52) Abramczyk, H.; Brozek-Pluska, B. New Look inside Human Breast Ducts with Raman Imaging. Raman Candidates as Diagnostic Markers for Breast Cancer Prognosis: Mammaglobin, Palmitic Acid and Sphingomyelin. *Anal Chim Acta* **2016**, *909*, 91–100. https://doi.org/10.1016/j.aca.2015.12.038.

(53) Hajab, H.; Anwar, A.; Nawaz, H.; Majeed, M. I.; Alwadie, N.; Shabbir, S.; Amber, A.; Jilani, M. I.; Nargis, H. F.; Zohaib, M.; Ismail, S.; Kamal, A.; Imran, M. Surface-Enhanced Raman Spectroscopy of the Filtrate Portions of the Blood Serum Samples of Breast Cancer Patients Obtained by Using 30 KDa Filtration Device. *Spectrochim Acta A Mol Biomol Spectrosc* **2024**, *311*, 124046. https://doi.org/10.1016/j.saa.2024.124046.

(54) Werner, S.; Keller, L.; Pantel, K. Epithelial Keratins: Biology and Implications as Diagnostic Markers for Liquid Biopsies. *Mol Aspects Med* **2020**, *72*, 100817. https://doi.org/10.1016/j.mam.2019.09.001.

(55) Vernuccio, F.; Vanna, R.; Ceconello, C.; Bresci, A.; Manetti, F.; Sorrentino, S.; Ghislanzoni, S.; Lambertucci, F.; Motiño, O.; Martins, I.; Kroemer, G.; Bongarzone, I.; Cerullo, G.; Polli, D. Full-Spectrum CARS Microscopy of Cells and Tissues with Ultrashort White-Light Continuum Pulses. *J Phys Chem B* **2023**, *127* (21), 4733–4745. https://doi.org/10.1021/acs.jpcb.3c01443.

(56) De la Cadena, A.; Vernuccio, F.; Ragni, A.; Sciortino, G.; Vanna, R.; Ferrante, C.; Pediconi, N.; Valensise, C.; Genchi, L.; Laptenok, S. P.; Doni, A.; Erreni, M.; Scopigno, T.; Liberale, C.; Ferrari, G.; Sampietro, M.; Cerullo, G.; Polli, D. Broadband Stimulated Raman Imaging Based on Multi-Channel Lock-in Detection for Spectral Histopathology. *APL Photonics* **2022**, *7* (7). https://doi.org/10.1063/5.0093946.

(57) Meyer, T.; Chemnitz, M.; Baumgartl, M.; Gottschall, T.; Pascher, T.; Matthäus, C.; Romeike, B. F. M.; Brehm, B. R.; Limpert, J.; Tünnermann, A.; Schmitt, M.; Dietzek, B.; Popp, J. Expanding Multimodal Microscopy by High Spectral Resolution Coherent Anti-Stokes Raman Scattering Imaging for Clinical Disease Diagnostics. *Anal Chem* **2013**, *85* (14), 6703–6715. https://doi.org/10.1021/ac400570w.

(58) Dreissig, I.; Machill, S.; Salzer, R.; Krafft, C. Quantification of Brain Lipids by FTIR Spectroscopy and Partial Least Squares Regression. *Spectrochim Acta A Mol Biomol Spectrosc* **2009**, *71* (5), 2069–2075. https://doi.org/10.1016/j.saa.2008.08.008.

(59) Elkins, K. M. Rapid Presumptive "Fingerprinting" of Body Fluids and Materials by ATR FT-IR Spectroscopy* ,†. *J Forensic Sci* **2011**, *56* (6), 1580–1587. https://doi.org/10.1111/j.1556-4029.2011.01870.x.

View Article Online
DOI: 10.1039/D4AN00868E

## Data availability

The data supporting this article have been included as part of the Supplementary Information.